Article

Cell Reports

STAT3 and STAT6 Signaling Pathways Synergize to Promote Cathepsin Secretion from Macrophages via IRE1α Activation

Graphical Abstract

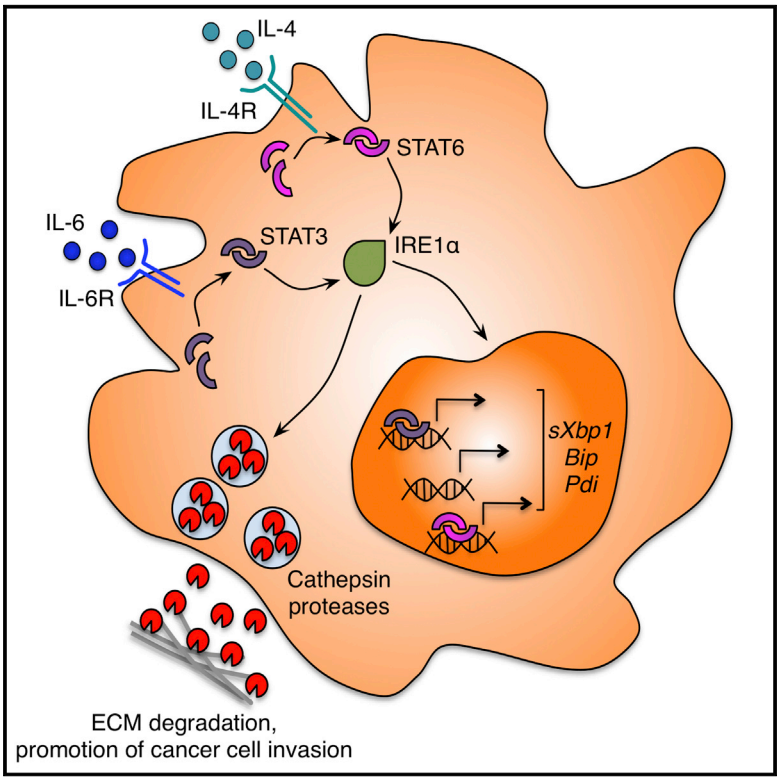

Highlights

- STAT3 and STAT6 cooperation in tumor-associated macrophages promotes tumor progression
- IL-4 synergizes with IL-6 and IL-10 to enhance cathepsin secretion via STAT3 and STAT6
- Cytokine synergy reshapes transcriptome, notably unfolded protein response (UPR) genes
- STAT3 and STAT6 regulate cathepsin secretion and UPR expression via IRE1α

Authors

Dongyao Yan, Hao-Wei Wang, Robert L. Bowman, Johanna A. Joyce

Correspondence

johanna@joycelab.org

In Brief

Yan et al. report that the T_H2 cytokine IL-4 synergizes with IL-6 and IL-10 in macrophages to promote pancreatic neuroendocrine tumor growth and invasion. The authors show that such synergy depends on STAT3 and STAT6 interaction to activate IRE1α, leading to a pronounced secretion of cathepsin proteases and induction of unfolded protein response-related genes.

Accession Numbers

GSE70626

Yan et al., 2016, Cell Reports *16*, 2914–2927
September 13, 2016 © 2016 The Author(s).
http://dx.doi.org/10.1016/j.celrep.2016.08.035

OPEN ACCESS
CellPress

Cell Reports
Article

STAT3 and STAT6 Signaling Pathways Synergize to Promote Cathepsin Secretion from Macrophages via IRE1α Activation

Dongyao Yan,[1,4] Hao-Wei Wang,[1,4] Robert L. Bowman,[1,4] and Johanna A. Joyce[1,2,3,5,*]
[1]Cancer Biology and Genetics Program, Memorial Sloan-Kettering Cancer Center, New York, NY 10065, USA
[2]Ludwig Institute for Cancer Research
[3]Department of Oncology
University of Lausanne, 1066 Lausanne, Switzerland
[4]Co-first author
[5]Lead Contact
*Correspondence: johanna@joycelab.org
http://dx.doi.org/10.1016/j.celrep.2016.08.035

SUMMARY

Tumor-associated macrophages play critical roles during tumor progression by promoting angiogenesis, cancer cell proliferation, invasion, and metastasis. Cysteine cathepsin proteases, produced by macrophages and cancer cells, modulate these processes, but it remains unclear how these typically lysosomal enzymes are regulated and secreted within the tumor microenvironment. Here, we identify a STAT3 and STAT6 synergy that potently upregulates cathepsin secretion by macrophages via engagement of an unfolded protein response (UPR) pathway. Whole-genome expression analyses revealed that the T_H2 cytokine interleukin (IL)-4 synergizes with IL-6 or IL-10 to activate UPR via STAT6 and STAT3. Pharmacological inhibition of the UPR sensor IRE1α blocks cathepsin secretion and blunts macrophage-mediated cancer cell invasion. Similarly, genetic deletion of STAT3 and STAT6 signaling components impairs tumor development and invasion in vivo. Together, these findings demonstrate that cytokine-activated STAT3 and STAT6 cooperate in macrophages to promote a secretory phenotype that enhances tumor progression in a cathepsin-dependent manner.

INTRODUCTION

Tumor-associated macrophages (TAMs) play critical roles in multiple stages of tumorigenesis and also contribute to chemoresistance (Quail and Joyce, 2013; Noy and Pollard, 2014; Ruffell and Coussens, 2015). Through reciprocal interactions with cancer cells and immune cell infiltrates, TAMs sculpt the tumor microenvironment (TME) to regulate critical aspects of tumor progression, including local inflammation, angiogenesis, cancer cell invasion, and intravasation into the circulation (Qian and Pollard, 2010). At the molecular level, this is achieved via a wide range of TAM-derived cytokines, growth factors, and proteases that mediate autocrine/paracrine signaling as well as modifications to the extracellular matrix (ECM). These factors often enhance the malignant phenotype of cancer cells and, thus, impart additional advantages to these cells within the TME. Therefore, understanding how TAM-derived factors interact and collectively regulate cancer cell behavior is essential for elucidating TAM biology and developing novel TAM-based therapies.

Among TAM-supplied proteases, members of the cysteine cathepsin family have been implicated in multiple aspects of carcinogenesis, including cancer cell proliferation, angiogenesis, invasion, and metastasis, in different tumor types (Olson and Joyce, 2015). Typically, cathepsins are synthesized as pro-form zymogens that can be activated in the acidic lysosomal compartment and, thus, execute intracellular degradation of proteins delivered to the lysosome (Turk et al., 2012). However, numerous studies have shown that several cathepsin family members also perform extra-lysosomal functions, such as antigen presentation (Riese et al., 1996), inflammasome activation (Hornung et al., 2008), and growth factor processing (Wiley et al., 1985). Importantly, when secreted into the extracellular space, these enzymes can degrade the ECM and basement membranes, cleave cell-adhesion molecules, and participate in proteolytic cascades, resulting in sequential protease activation, which collectively promotes tumor invasion and metastasis (Olson and Joyce, 2015). Therefore, elucidation of the molecular mechanisms governing the secretion and extracellular activities of cathepsins is critical.

Previously, we demonstrated that interleukin (IL)-4 signaling is, at least partially, responsible for inducing high cathepsin activity levels in TAMs, in addition to its role in controlling other facets of macrophage biology (Gocheva et al., 2010b; Wang and Joyce, 2010). However, as TAMs typically reside in complex TMEs composed of diverse cytokines, it remains to be determined whether other factors operate in concert with IL-4 to mediate coordinated responses. Indeed, aside from IL-4, other cytokines, including IL-13, IL-6, and IL-10, readily activate macrophages (Biswas and Mantovani, 2010). It has recently been reported

 © 2016 The Author(s).
This is an open access article under the CC BY-NC-ND license (http://creativecommons.org/licenses/by-nc-nd/4.0/).

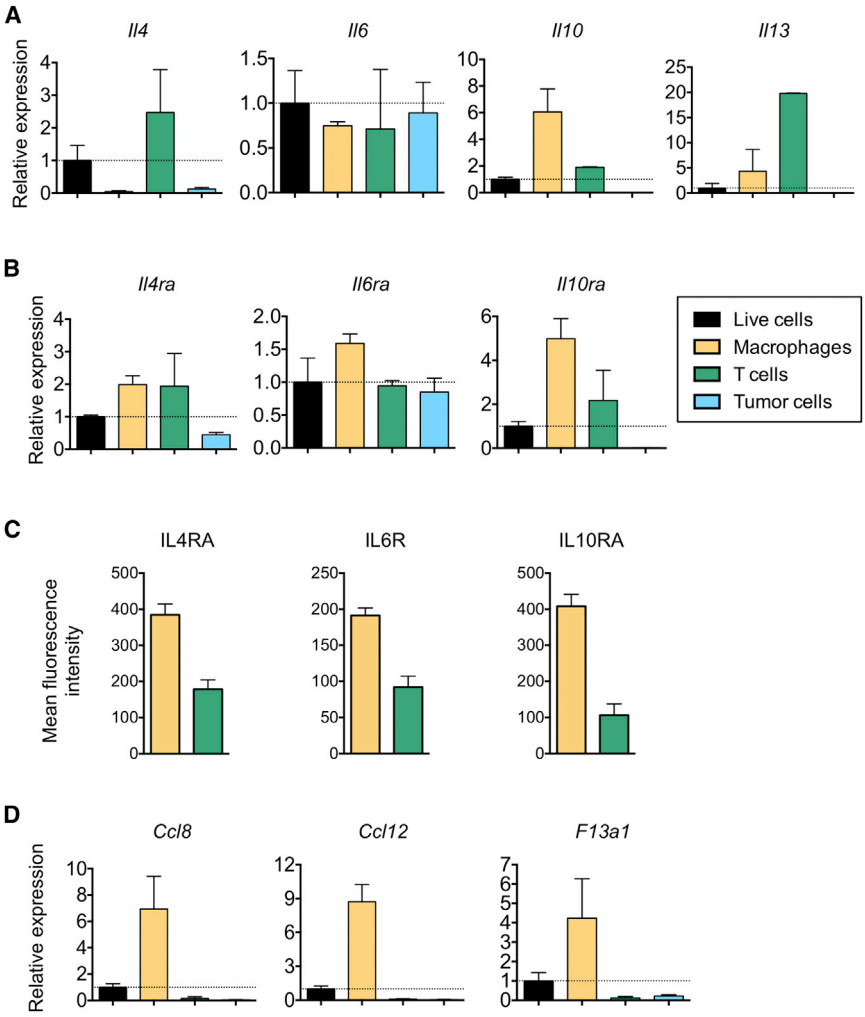

Figure 1. Expression of T_H2-Associated Cytokine Signaling Molecules in Constituent Cell Types within the RT2 Tumor Microenvironment

(A and B) Gene expression in mixed live cells or FACS-purified macrophages ($CD45^+$, $F4/80^+$, $GR.1^-$), T cells ($CD45^+$, $CD3^+$, $GR.1^-$), and cancer cells ($CD45^-$, $CD31^-$) from wild-type (WT) RT2 tumors was analyzed by qRT-PCR for (A) *Il4*, *Il6*, *Il10*, and *Il13*; and (B) *Il4ra*, *Il6ra*, and *Il10ra*.

(C) Mean fluorescence intensities of IL4RA, IL6R, and IL10RA protein levels were assessed by flow cytometry in macrophages and T cells isolated from RT2 tumors.

(D) Expression of *Ccl8*, *Ccl12*, and *F13a1* was analyzed by qRT-PCR.

Data are presented as mean ± SEM of expression; levels are relative to the mixed live-cell population from n = 3 independent biological replicates. The relative expression level of the live-cell population is set to 1 and denoted by the dotted line. See also Figure S1.

that several T_H2-associated cytokines coordinately activate STAT6 (the downstream effector of IL-4 and IL-13) and STAT3 (the downstream effector of IL-6 and IL-10) to regulate T_H2 cell differentiation (Stritesky et al., 2011), suggesting a crosstalk mechanism responsive to multiple cytokine inputs. However, it is currently unknown whether similar machinery also operates in macrophages to modulate their activation and functions.

To address this question, we have used genetic approaches to demonstrate that both STAT3 and STAT6 signaling critically contribute to tumor development and cancer cell invasion in vitro and in vivo. We determined that STAT3/STAT6-activating cytokines cooperate to regulate cathepsin expression and, more potently, secretion in bone marrow (BM)-derived macrophages (BMDMs). Whole-genome expression analyses revealed that combined cytokine treatment of BMDMs led to pronounced transcriptional reprogramming highlighted by the upregulation of secretion-associated genes. Furthermore, we found that the synergistic induction of the secretion of pro-cathepsins is predominately regulated by activation of the inositol-requiring enzyme 1α (IRE1α) axis of the unfolded protein response (UPR) pathway.

RESULTS

Genetic Deletion of Components of the STAT3 and STAT6 Cytokine Signaling Pathways Impairs Tumorigenesis

TAMs reside in complex microenvironments that are typically T_H2 skewed (Biswas and Mantovani, 2010; Shiao et al., 2011). Previously, we showed that the T_H2 cytokine IL-4, which is progressively upregulated during pancreatic neuroendocrine tumor (PanNET) development in the RIP1-Tag2 (RT2) mouse model, is an important inducer of high global cysteine cathepsin activity in TAMs, which peaks in the most invasive of RT2 tumors (Gocheva et al., 2010b). However, in this earlier study, we did not address whether the overall increase in pan-cathepsin activity was the result of transcriptional, translational, or localization changes in specific cysteine cathepsin family members, of which there are 11 in humans (Turk et al., 2012). Moreover, given that *Il4* deletion only reduced the proportion of cathepsin-activity-high TAMs by approximately 40% (Gocheva et al., 2010b), additional cytokines in the TME are likely to regulate this important phenotype of TAMs.

To directly interrogate T_H2-associated cytokine signaling programs in vivo, we first quantified the expression levels of the signaling components in individual cell populations within the PanNET TME. We used fluorescence-activated cell sorting (FACS) to isolate TAMs, T cells, and cancer cells, based on their distinct patterns of surface marker expression. Separation of pure cell populations was confirmed by exclusive expression of *Cd68* in macrophages, *Cd3e* in T cells, and SV40-*Tag* in cancer cells (Figure S1A). qRT-PCR analysis showed that *Il4*, *Il10*, and *Il13* were mainly expressed in T cells or TAMs, while *Il6* was uniformly expressed across all cell populations (Figure 1A).

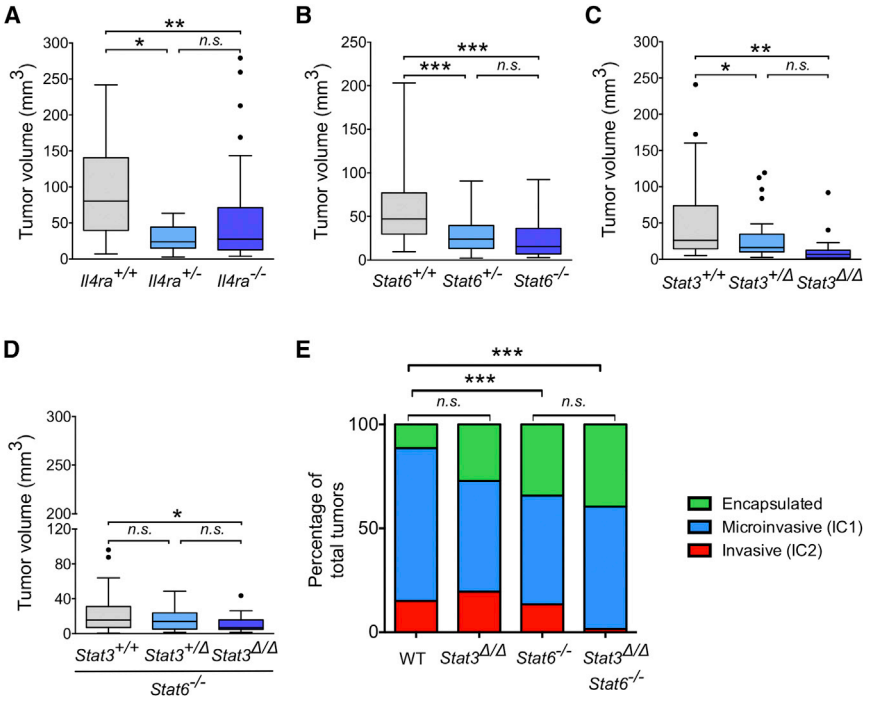

Figure 2. Genetic Deletion of STAT3 and STAT6 Signaling Pathways Blunts RT2 Tumor Development and Invasion

(A and B) RT2 mice developed multiple tumors by the end-stage 13.5-week time point, and cumulative tumor volume was determined for each genotype. Mice with constitutive deletion of (A) *Il4ra* (n = 24 for *Il4ra*$^{+/-}$; n = 40 for *Il4ra*$^{-/-}$) or (B) *Stat6* (n = 48 for *Stat6*$^{+/-}$; n = 39 for *Stat6*$^{-/-}$) were compared with the corresponding littermate controls (n = 31 for *Il4ra* cohorts; n = 57 for *Stat6* cohorts).

(C) The cumulative tumor volume in each RT2 mouse with conditional deletion of *Stat3* by *LysM*:Cre (n = 39 for *Stat3*$^{+/\Delta}$; n = 21 for *Stat3*$^{\Delta/\Delta}$) was determined at 13.5 weeks of age and compared with the corresponding littermate controls (n = 34).

(D) Tumor volume plot shows the double-knockout RT2 mice with constitutive deletion of *Stat6* and *LysM*:Cre-mediated deletion of *Stat3*. Tumor volumes (n = 47 for *Stat3*$^{+/\Delta}$ *Stat6*$^{-/-}$; n = 17 for *Stat3*$^{\Delta/\Delta}$ *Stat6*$^{-/-}$) were compared with littermate controls (n = 54). Tukey box-and-whisker plots are shown in (A–D) with values outside the whiskers. All data points were included in statistical analyses. All comparisons of tumor volumes were analyzed using Kruskal-Wallis tests with Dunn's multiple comparisons.

(E) H&E staining was performed, and tumors from *Stat3*$^{\Delta/\Delta}$ (n = 11), *Stat6*$^{-/-}$ (n = 10), *Stat6*$^{-/-}$-*Stat3*$^{\Delta/\Delta}$ (n = 9), and WT littermates (n = 13) were classified into three categories: encapsulated (green), microinvasive (IC1, blue), and invasive (IC2, red). The relative proportions of the three categories in each genotype are shown in each column. The distributions of tumor invasion were compared using a cumulative logit model with generalized estimating equations to correct for correlations within individual mice. *$p < 0.05$; **$p < 0.01$; ***$p < 0.001$; n.s., non-significant.

Specifically, T cells expressed the highest levels of *Il4* and *Il13*, whereas *Il10* expression was most prominent in macrophages (Figure 1A). TAMs expressed the corresponding cytokine receptors at both the mRNA and protein levels (Figures 1B and 1C), as well as the downstream transcriptional mediators *Stat3* (for IL-6 and IL-10) and *Stat6* (for IL-4 and IL-13) (Figure S1B). We found that TAMs expressed high levels of genes associated with an IL-4-driven alternative-activation phenotype, including *Ccl8* (Hiwatashi et al., 2011), *Ccl12*, and *F13a1* (Ostuni et al., 2013), indicating the capacity of TAMs to receive the T_H2 cytokine inputs (Figure 1D).

We next examined the role of T_H2-associated cytokine signaling in tumor development by genetically deleting multiple components of the IL-4 signaling axis in the RT2 model. End-stage analysis at 13.5 weeks revealed that mice with constitutive deletion of the *Il4ra* receptor led to a significant decrease in tumor burden compared to wild-type (WT) RT2 animals (Figure 2A). Genetic deletion of *Stat6,* the critical downstream mediator of IL-4Rα signaling, also resulted in a significant decrease in cumulative tumor volume (Figure 2B). Because heterozygous *Stat6* deletion resulted in a similar reduction in tumor burden, compared to *Stat6* homozygous knockouts (Figure 2B), we sought to determine whether *Stat6*$^{+/-}$ BMDMs still respond to IL-4 stimulation (Figure S1C). Our data suggest that, while *Stat6*$^{+/-}$ BMDMs retained some responsiveness to IL-4, the magnitude of IL-4-mediated activation was significantly attenuated, as indicated by the diminished induction of *Arg1*, *Ccl22*, *Ccl8*, and *Ccl12* (Figure S1C). Therefore, the reduction of tumor volume observed in *Stat6*$^{+/-}$ RT2 mice may be the result of partial *Stat6* loss in both TAMs and tumor cells.

To define the contribution of BM-derived cells to these phenotypes, we performed BM transplantation (BMT) experiments. We have previously shown that the vast majority (88%) of BM-derived cells in RT2 tumors differentiate into TAMs (Gocheva et al., 2010b); thus, BMT provides a strategy to experimentally manipulate the expression of TAM-supplied factors such as STAT6 in vivo. We transferred WT or *Stat6*$^{-/-}$ donor BM into lethally irradiated WT RT2 recipients at 4 weeks of age and subsequently assessed end-stage tumor volume at 13.5 weeks. Mice transplanted with *Stat6*$^{-/-}$ BM showed a markedly lower tumor burden compared to WT BM counterparts (Figure S1D). Together, these findings demonstrate that the IL-4/ STAT6 signaling pathway critically contributes to tumor development.

The presence of intratumoral STAT3-activating cytokines (IL-6 and IL-10) in the TME prompted us to also delineate the role of STAT3 in PanNET development. *Stat3*-deficient animals are embryonic lethal (Takeda et al., 1997); therefore, we conditionally deleted *Stat3* in myeloid cells of RT2 mice using the *LysM*:Cre line (here after termed *Stat3*$^{\Delta/\Delta}$) (Takeda et al., 1999). Mice with a heterozygous or homozygous *Stat3* deletion showed a significantly lower tumor burden compared to WT RT2 (Figure 2C). To next determine whether *Stat6* and *Stat3* act in an additive or epistatic manner, we generated *Stat6*$^{-/-}$ RT2 mice with either a heterozygous or a homozygous *Stat3* deletion in myeloid cells

and analyzed end-stage tumor burden. Compared to *Stat6*$^{-/-}$ mice, animals with an additional *Stat3* deletion had significantly lower tumor volume (Figure 2D). Collectively, these genetic experiments show that STAT6 and STAT3 synergistically regulate PanNET progression in vivo.

STAT3 and STAT6 Signaling Enhance Tumor Invasion

Previously, we have shown that IL-4 increases pan-cathepsin activity in TAMs and that TAMs, in turn, promote cancer cell invasion (Gocheva et al., 2010b). Therefore, we examined the effect of genetically ablating STAT3/STAT6 signaling components on tumor invasiveness in vivo. Based on histological features, RT2 tumors are classified into encapsulated tumors, microinvasive carcinomas (IC1), and frankly invasive carcinomas (IC2), as previously described (Lopez and Hanahan, 2002; Gocheva et al., 2010b). WT RT2 tumors comprise all three grades, with IC1 being the predominant type. To determine the impact of STAT6 and STAT3 on tumor invasion, we compared *Stat6*$^{-/-}$ tumors, *Stat3*$^{\Delta/\Delta}$ tumors, and *Stat6*$^{-/-}$ *Stat3*$^{\Delta/\Delta}$ tumors with their WT counterparts. *Stat6* deletion significantly impaired tumor invasion compared to WT. While deletion of *Stat3* also trended toward reduced tumor invasion, this was not statistically significant compared to WT tumors (Figure 2E). Similarly, the combined ablation of both *Stat6* and *Stat3* did not further decrease tumor invasion compared to *Stat6* deletion alone, though there was a trend toward less IC2-invasive tumors. In sum, these results suggest that perturbation of the STAT6 signaling pathway is sufficient to limit the invasive capacity of tumors.

STAT3/STAT6-Activating Cytokines Cooperate to Regulate Cathepsin Transcription and Secretion by Macrophages

Given that STAT3 and STAT6 cooperate during T_H2 cell development (Stritesky et al., 2011), and given their synergistic functions in promoting RT2 tumor growth and invasion (Figure 2), we hypothesized that concurrent activation of STAT6 and STAT3 could potently enhance the pro-tumorigenic functions of macrophages. We specifically focused on macrophage-derived cathepsins, because abundant evidence has established their importance in PanNET progression and invasion (Joyce et al., 2004; Gocheva et al., 2006, 2010a, 2010b; Akkari et al., 2014, 2016). We first stimulated BMDMs with either IL-4 alone or a "cytokine cocktail" (comprising IL-4, IL-6, IL-10, and IL-13) for 6 consecutive days. We specifically analyzed expression of the 6 of 11 cathepsin family members (*CtsB*, *C*, *H*, *L*, *S*, and *Z*) that we had previously shown to be upregulated during multistage RT2 tumorigenesis (Joyce et al., 2004). Expression analysis demonstrated modest additional upregulation of *CtsB*, *CtsC*, *CtsS*, and *CtsZ* mRNA after combined cytokine stimulation compared to IL-4 stimulation alone (Figure 3A). The mRNA level of *CtsL*, however, was dramatically elevated by the cytokine cocktail compared to IL-4 (Figure 3A). *CtsH* was the only family member that did not show further enhanced expression by combined cytokines (Figure 3A). These findings highlight the differential transcriptional regulation of cathepsin family members following T_H2-associated cytokine treatment.

Next, we analyzed the levels of secreted cathepsins under individual and combinatorial cytokine conditions using macrophage-conditioned media (CM) labeled with DCG-04 (Greenbaum et al., 2000), a pan-cathepsin probe that has been widely used to assay cathepsin abundance and activity (e.g., Joyce et al., 2004; Rooney et al., 2005; Vasiljeva et al., 2006; Chandramohanadas et al., 2009). While IL-4 and the other T_H2-associated cytokines increased pan-cathepsin secretion, the "cocktail" treatment resulted in the most robust response (Figure 3B), with all treatments leading to some increase in overall protein secretion compared to controls (Figure S2A). Interestingly, a substantial proportion of cathepsins were secreted as pro-forms, as indicated by the alterations of their molecular weights following incubation in cathepsin activation buffer (Figure 3B). Western blots for individual cathepsins confirmed that combined cytokine treatment robustly upregulated the secretion of CtsB, CtsL, CtsS, and CtsZ (Figure S2B). Compared with single cytokines, combined cytokines also triggered upregulation of intracellular CtsL protein but not the other cathepsins (Figure S2C), which corresponds to the pronounced transcriptional induction of *CtsL* (Figure 3A). By contrast, discordance between transcriptional and secretory regulation is highlighted by the lack of alteration in CtsC secretion following combined cytokine treatment (Figure S2B), despite a modest increase at the mRNA level (Figure 3A). Cathepsin secretion was more potent with IL-4, as IL-13 did not further promote cathepsin secretion when combined with IL-6 or IL-10 (Figures S3A–S3D). These results demonstrate that cathepsin abundance and localization are differentially regulated by T_H2-associated cytokines, with secretion being the most prominent effect.

To gain further insight into these regulatory complexities, we focused on the downstream mediators of T_H2 cytokine signaling, STAT6 and STAT3. We combined IL-4 with either IL-6 or IL-10 to non-redundantly stimulate WT, *Stat6*$^{-/-}$, or *Stat3*$^{\Delta/\Delta}$ BMDMs. Both cytokine combinations resulted in a synergistic upregulation of cathepsin secretion by WT BMDMs, which was abolished by *Stat6* or *Stat3* inactivation (Figure 3C). Taken together, our data suggest that both STAT6 and STAT3 are required for the T_H2-associated cytokine-induced synergistic secretion of cathepsins by macrophages.

Combined Cytokine Stimulation Reshapes the Transcriptional Landscape of Macrophages toward a Secretory Phenotype

We determined that, although STAT6 and STAT3 were capable of mediating cathepsin transcription, their direct transcriptional regulation was modest and, therefore, not sufficient to explain the greater magnitude of the enhanced secretory phenotype for several cathepsin family members. We reasoned that additional STAT6 and STAT3 targets might mediate the synergistic cathepsin secretion from stimulated BMDMs. Therefore, we performed whole-genome expression profiling to gain systematic insights into cytokine-mediated transcriptional changes in macrophages. Principal-component analysis (PCA) revealed that IL-4 induced a distinct repertoire of transcriptional changes in BMDMs, compared with IL-6 or IL-10, and combined cytokines modified the transcriptional landscape differently from single cytokines (Figure 4A). When analyzing the interactions between IL-4 and IL-6, we defined six patterns of gene expression: (I) genes upregulated by IL-4 but not by IL-6 or the combination

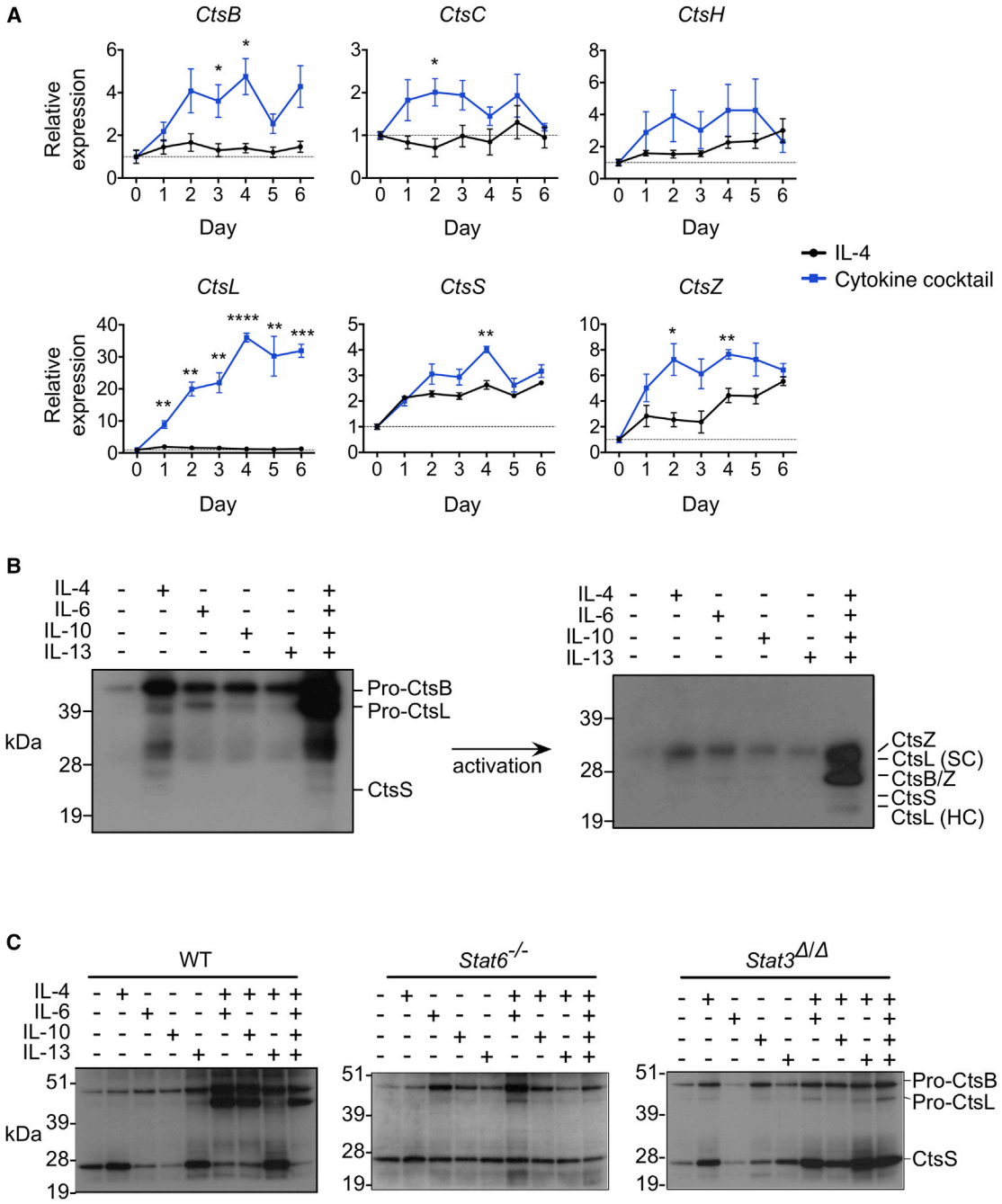

Figure 3. T_H2-Associated Cytokines Synergize to Enhance Cathepsin Expression and Pro-form Cathepsin Secretion in a STAT3- and STAT6-Dependent Manner

(A) Wild-type bone marrow-derived macrophages (BMDMs) were stimulated with either IL-4 (10 ng/ml) alone or a "cytokine cocktail" (including IL-4, IL-6, IL-10, and IL-13; 10 ng/ml each) for up to 6 consecutive days. The transcripts of *CtsB*, *CtsC*, *CtsH*, *CtsL*, *CtsS*, and *CtsZ* were quantified by qRT-PCR. Data are shown as the mean ± SEM of n = 3 independent experiments. One-way ANOVA, followed by Fisher's least significant difference (LSD), test was used to assess significance between IL-4 and the "cytokine cocktail" treatment group.

(B) BMDMs were stimulated with indicated cytokines for 48 hr, followed by 24-hr conditioning in serum-free media. Equal volumes of conditioned media (CM) were then labeled with the cathepsin probe DCG-04 and analyzed by immunoblotting (left). In parallel, CM was activated in vitro, using cathepsin activation buffer, and subsequently labeled with DCG-04. Immunoblotting was performed to assess cathepsin levels (right). SC, single chain; HC, heavy chain.

(C) BMDMs derived from WT, *Stat6*$^{-/-}$, and *Stat3*$^{\Delta/\Delta}$ mice were stimulated with individual or combinatorial cytokines (10 ng/ml each) for 48 hr and then cultured in serum-free media for 24 hr to generate CM. CM were then labeled with DCG-04, followed by immunoblotting. Results are representative of n = 3 independent biological replicates. "Pro-" indicates pro-form. Protein sizes (in kilodaltons) are indicated on the left of each blot. *$p < 0.05$; **$p < 0.01$; ***$p < 0.001$; ****$p < 0.0001$. See also Figures S2 and S3.

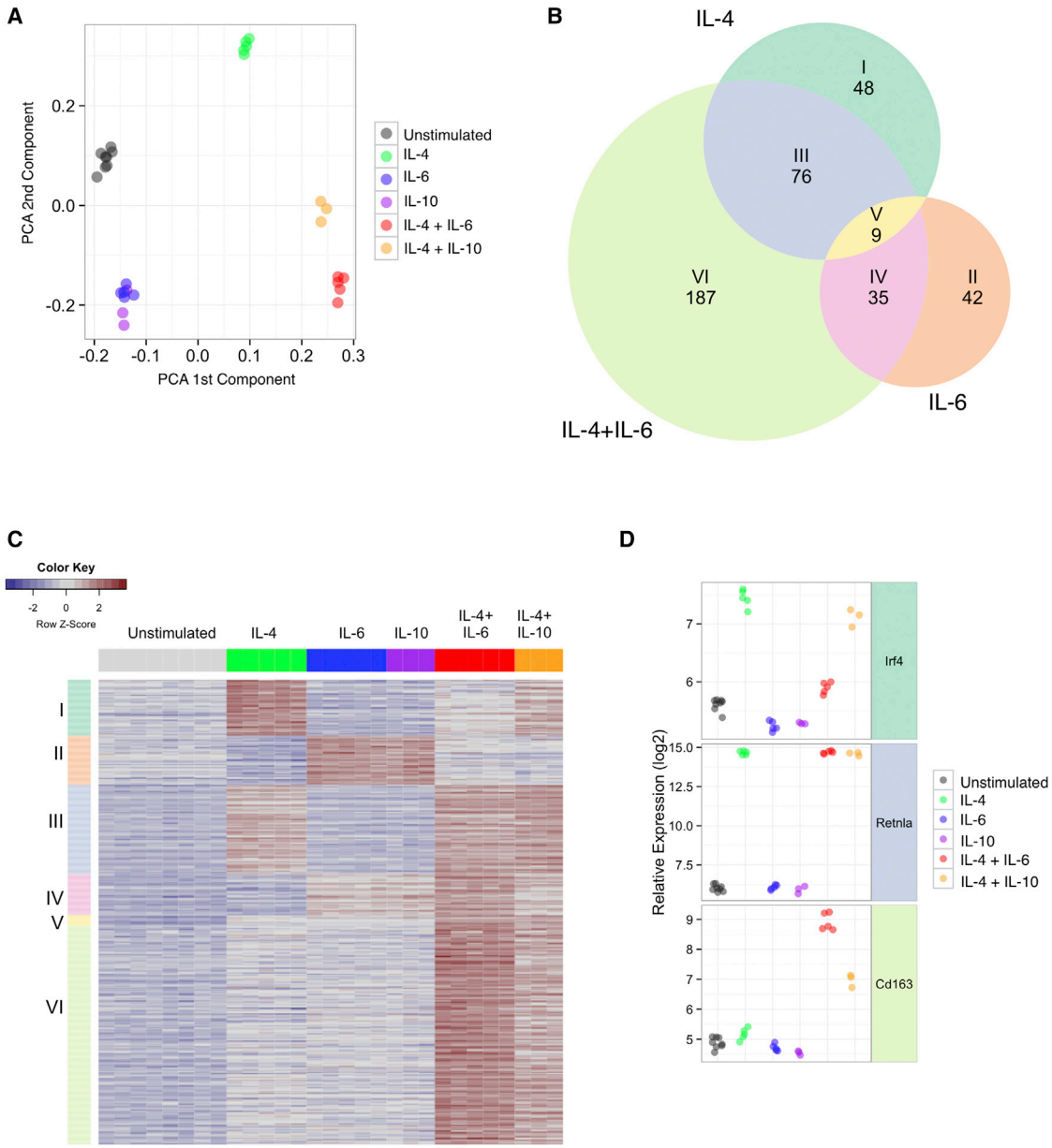

Figure 4. Combined Cytokine Stimulation Elicits Non-additive Transcriptional Programs

BMDMs were either untreated or treated for 24 hr with IL-4, IL-6, IL-10, IL-4 + IL-6 together, or IL-4 + IL-10. RNA was isolated, and gene expression changes were assessed by microarrays.

(A) Principal-component analysis (PCA) of gene expression data shows clear separation of the combined-cytokine from the single-cytokine treatment group. Each dot represents a biological replicate for the indicated treatment group. The first principal component (PC) is shown on the x axis, and the second PC is shown on the y axis, accounting for 52% and 19% of the total variance, respectively.

(B) Venn diagram of upregulated genes in IL-4 versus unstimulated, IL-6 versus unstimulated, and combined IL-4 + IL-6 versus unstimulated conditions. Six patterns of expression for upregulated genes were identified, and the numbers of genes are indicated for each pattern (fold change ± 2, FDR 0.05%): (I) genes upregulated by IL-4 but not by IL-6 or the combination of IL-4 + IL-6; (II) genes upregulated by IL-6 but not by IL-4 or the combination of IL-4 + IL-6; (III) genes upregulated by IL-4 and by IL-4 + IL-6 together but not by IL-6 alone; (IV) genes upregulated by IL-6 and by IL-4 + IL-6 but not by IL-4 alone; (V) genes upregulated by IL-4, IL-6, and the combination of IL-4 + IL-6; and (VI) genes responsive only to the combination of IL-4 + IL-6.

(C) Heatmap of genes corresponding to the Venn diagram in (B).

(D) Log_2 gene expression values (microarray) for *Irf4*, *Retnla*, and *Cd163*.

See also Figure S4 and Table S1.

of IL-4 + IL-6; (II) genes upregulated by IL-6 but not by IL-4 or the combination of IL-4 + IL-6; (III) genes upregulated by IL-4 and by IL-4 + IL-6 together but not by IL-6 alone; (IV) genes upregulated by IL-6 and by IL-4 + IL-6 but not by IL-4 alone; (V) genes upregulated by IL-4, IL-6, and the combination of IL-4 + IL-6; and (VI) genes responsive only to the combination of IL-4 + IL-6 (Figure 4B; complete gene expression results can be found in Table S1). We found 133 genes upregulated by IL-4 treatment, including well-known responsive genes such as *Arg1*, *Ccl17*, *Ccl22*, and *Irf4* (El Chartouni et al., 2010; Wang and Joyce, 2010) (Figures 4B and 4C). In addition we found that both IL-6 and IL-4 + IL-6 stimulation induce *Il4ra* (Figures 4B, 4C, and S4B), a finding previously proposed to support the role of IL-6 in alternative macrophage activation (Mauer et al., 2014). Moreover, 187 genes (pattern IV, including *Cd163*, *Cd209a/ DC-SIGN*, and *Cd274/ PD-L1*) were upregulated by IL-4 + IL-6 in combination but showed no response to either cytokine alone (Figures 4B and 4C). These data highlight that cytokine interactions result in complex changes in the transcriptome in a non-additive manner.

In accordance with PCA, we found that there was considerable transcriptional similarity between IL-6-stimulated and IL-10-stimulated BMDMs, with only *Rsad2* and *Ifit3* being specifically upregulated in IL-6-treated macrophages (Figures 4A and S4A). Despite such a substantial overlap in transcriptional regulation, concurrent IL-4 stimulation dramatically amplified the differences between IL-6 and IL-10, with many more genes being differentially regulated in the combination conditions (Figures 4A, S4A, and S4B). Specifically we found 33 genes upregulated by combined IL-4 + IL-6, compared to IL-4 + IL-10, including *Il4ra, Socs3*, and *Cd209a* (Figures 4C, S4A, and S4B). Meanwhile, 13 genes were upregulated in response to combined IL-4 + IL-10 compared to IL-4 + IL-6, including *Ccl17*, *Ccl22*, and *Irf4* (Figures 4C and S4B). These findings demonstrate the non-redundancy of the two STAT3-activating cytokines IL-6 and IL-10 when combined with IL-4 stimulation.

To comprehensively assess these complex cytokine interactions, we used an interaction-based linear model to statistically quantify the extent to which target genes were regulated by single and combination cytokine treatments (Ritchie et al., 2015). This approach allowed us to more accurately distinguish IL-4-responsive genes (pattern III) from exclusively IL-4 + IL-6-responsive genes (pattern VI) for broader gene ontology (GO) analyses. In the most extreme cases, "induced" genes (n = 82) showed minimal response to single cytokines but striking increases in gene expression upon combined cytokine stimulation (Figure 5A). Conversely, "repressed" genes (n = 61) showed the opposite trend, where either of the combined cytokine treatments led to a decrease in expression (Figure 5A). In addition, we observed globally that the magnitude of synergy was most pronounced in the combined IL-4 + IL-6 condition, whereas IL-4 + IL-10 treatment led to a modest response (Figure S4C), confirming the trends observed for individual genes (Figure 4D). We next sought to summarize these global changes in gene expression using GO analysis. We focused on the combined IL-4 + IL-6 interaction term to assign a "synergy score" to each gene and assessed GO enrichment using iPAGE (Goodarzi et al., 2009). Interestingly, GO analysis uncovered an enrichment of Golgi-vesicle trafficking for the genes with the highest synergy score (Figure 5B, far right column), which contains GO terms related to secretion, vesicle transport, and exocytosis (Figure S4D). These findings highlight the phenotypic switch of macrophages to a secretory state upon combined cytokine stimulation.

Combined Cytokine Treatment Activates the UPR

Given these findings, we next sought to understand the mechanisms regulating protease secretion following combined cytokine treatment. Having already identified a role for STAT6 and STAT3 in mediating cathepsin secretion (Figure 3C), we utilized MARA (Suzuki et al., 2009) to gain additional mechanistic insight into putative downstream pathways regulating this process. As expected, transcription factor (TF) motifs representing STAT6 and STAT3 demonstrated increased activity under both individual and combined cytokine conditions compared to the unstimulated condition (Figure S4E). We next focused our attention on TF motifs that demonstrated synergistic induction in response to combined cytokine treatment in order to identify pathways regulating secretion and vesicle trafficking-related processes. We identified eight TF motifs that were induced under the combined cytokine condition: NFE2, ATF6, Rfx-family members, HOXA5/ B5, NR1H4, ATF2, ARNT, and XBP1 (Figure 5C). Only XBP1 and ATF6 targets were enriched for Golgi vesicle-related GO terms (Figures 5C and 5D). Interestingly, these factors have been shown to be the major mediators of the UPR; XBP1, in particular, has been implicated in antibody secretion from plasma cells (Reimold et al., 2001; Osorio et al., 2014). Collectively, these analyses suggest that combined cytokine stimulation activates UPR-associated TFs in macrophages, potentially resulting in a phenotypic switch to a secretory state.

There are three arms of the classical UPR, mediated via IRE1α/ XBP1, PERK, and ATF6, respectively, which are critical for regulating protein aggregates, thereby preventing endoplasmic reticulum (ER) stress (Bettigole and Glimcher, 2015). We first analyzed *Xbp1* splicing, which serves as a readout of upstream IRE1α activation. Consistent with the TF MARA analyses, spliced-*Xbp1* (s*Xbp1*) was significantly upregulated under the combined cytokine conditions (Figures 6A and S5A). A time-course analysis of *Xbp1* splicing revealed induction as early as 2 hr post-stimulation, which peaked at 24 hr and remained elevated after 48 hr (Figure 6B). By contrast, *Stat6*$^{-/-}$ and *Stat3*$^{\Delta/\Delta}$ BMDMs showed either severely attenuated or no s*Xbp1* induction upon combined cytokine stimulation (Figures 6C, 6D, and S5A). Similar kinetics of IRE1α phosphorylation and its *Stat3/ Stat6* dependence were identified, indicating activation of this pathway (Figure S5B).

Next, we assessed activation of the PERK pathway, another arm of the UPR, which was modestly activated by combined cytokines (Figure 6E). To determine whether there was a functional contribution of the PERK pathway to cathepsin secretion, BMDMs were pre-incubated with a pharmacological inhibitor of PERK, GSK2606414, followed by cytokine stimulation. However, PERK inhibition did not significantly alter the synergistic cathepsin secretion induced by combined cytokines (Figure 6F). Finally, we examined the third component of the classical UPR, ATF6. Following IL-4 + IL-6 treatment, we did not detect robust

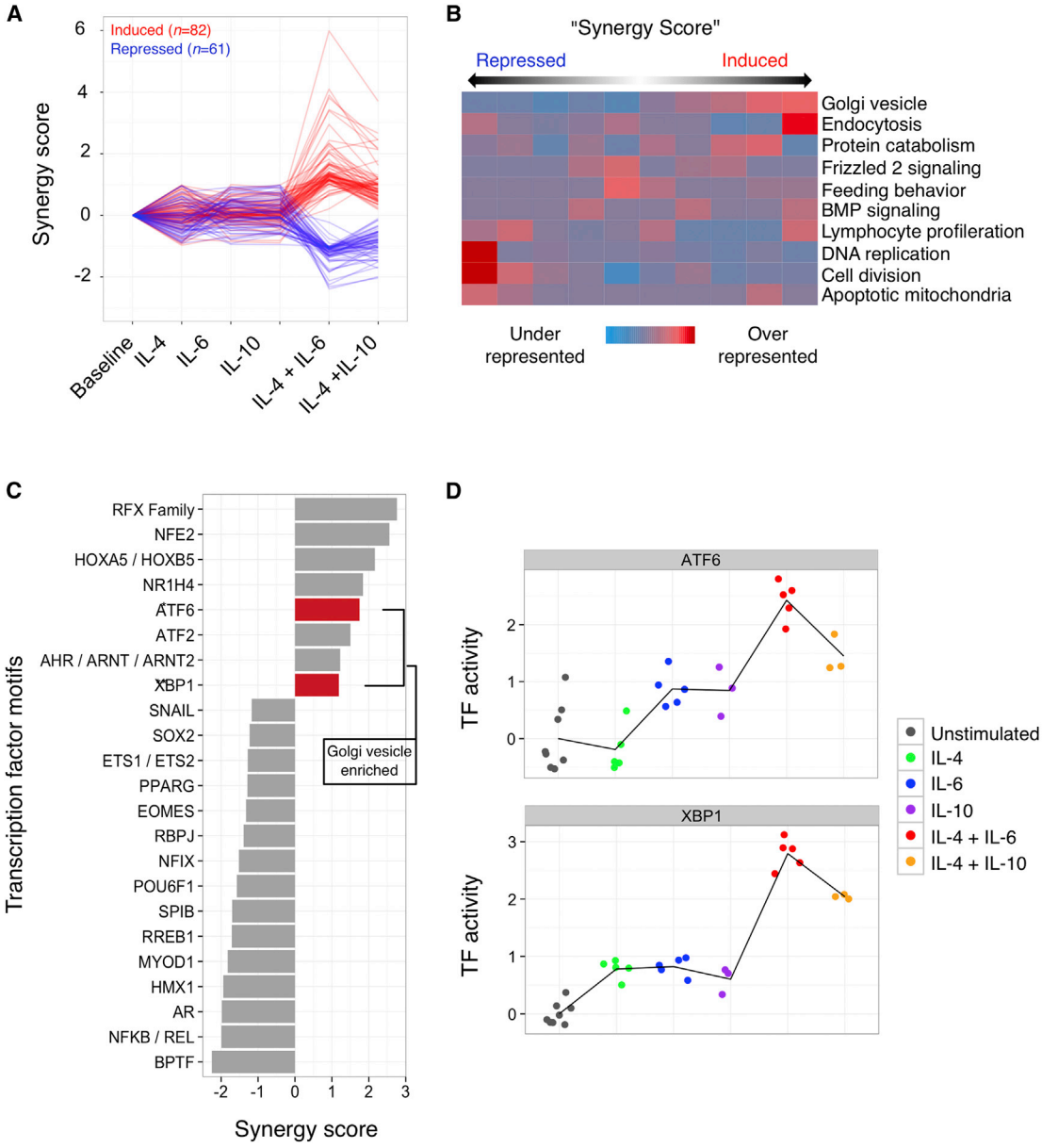

Figure 5. T_H2-Associated Cytokine Treatment Leads to Synergistic Gene Expression Changes and Engagement of the UPR

(A) Synergistic and antagonistic genes were identified using an interaction-based linear model as described in the Experimental Procedures. Log_2 coefficients for induced genes (n = 82) are plotted in red, and those for repressed genes (n = 61) are plotted in blue.

(B) The coefficient for the combined IL-4 + IL-6 interaction term in the linear model (A) was used to assign a "synergy score" to each gene. Genes were ranked based on "synergy score," and gene ontology (GO) analysis was completed using iPAGE. Over-represented and under-represented terms were scored using Fisher exact tests. Representations of the ensuing p values were plotted so that the overrepresented scores are shown in red and underrepresented scores are shown in blue.

(C) Transcription factor (TF) motif activity scores were generated using MARA. Synergistic activation of TF activity was identified using an interaction-based linear model, and the combined IL-4 + IL-6 interaction coefficient is shown here. GO enrichment for predicted TF targets was assessed in MARA. TF families enriched for "Golgi-vesicle-trafficking"-related GO terms are labeled in red (XBP1 and ATF6). A hypergeometric test was used for the statistical analysis of GO enrichment terms. $^*p < 0.05$; $^{**}p < 0.01$.

(D) Normalized model coefficients from (C) for XBP1 and ATF6, where each dot represents a biological replicate for the indicated treatment group.

See also Figure S4.

alterations in ATF cleavage or its nuclear localization (Figure 6E). When compared with UPR triggered by bona fide activators, including tunicamycin and thapsigargin, combined cytokine-mediated UPR shows modest induction of targets (Figures S5A and S6A). In addition, IL-4 is a more potent inducer of UPR than IL-13 when combined with IL-6 or IL-10 (Figure S6B).

Together, these findings suggest that T_H2-associated cytokines trigger an attenuated, non-canonical UPR in macrophages, which potentially leads to the secretory phenotype.

Inhibition of IRE1α Blocks Cathepsin Secretion and Macrophage-Driven Cancer Cell Invasion

Having excluded a role for PERK or ATF6 in controlling the secretory phenotype, we therefore sought to determine whether IRE1α was the key regulator. Transient small interfering RNA (siRNA)-mediated knockdown of IRE1α resulted in significant attenuation in UPR induction by combined cytokines (Figures S7A and S7B). We also used a small-molecule inhibitor of the RNase domain of IRE1α, STF-083010 (Papandreou et al., 2011), to assess the role of IRE1α in UPR induction in macrophages. We found that STF-083010 blocked cytokine-induced *Xbp1* splicing (Figure S7C) and sXBP1 protein abundance (Figure S7D), indicating functional inhibition of IRE1α. Similarly, the induction of UPR genes (*Bip* and *Pdi*) was also dependent upon IRE1α activity (Figure S7C).

We then investigated whether perturbation of IRE1α would blunt T_H2 cytokine-mediated cathepsin secretion. IRE1α knockdown completely abolished cathepsin secretion from BMDMs treated with combined cytokines (Figure 7A). This finding was further corroborated by using three independent IRE1α pharmacological inhibitors, STF-083010, 4μ8C, and KIRA6 (Figures 7B, S7E, and S7F). Interestingly, this phenomenon appears to extend beyond cathepsins, as secretion of the lysosomal enzyme legumain (LGMN) also depended on IRE1α activity (Figures 7A, 7B, S7E, and S7F). By contrast, the secretion of MMP9 and MMP13, two representative matrix metalloproteases (MMPs) produced in abundance by macrophages, was not synergistically regulated by combined cytokines, and IRE1α inhibition did not block MMP secretion (Figures 7A and 7B). Together, these findings indicate that IRE1α-dependent synergistic secretion of proteins from macrophages is specific to a subset of lysosomal proteases.

Our in vivo data suggest that TAMs can enhance tumor invasion. To investigate how cytokine signaling in TAMs promotes this process, we utilized a transwell invasion assay in which βTC374 cancer cells (a cell line derived from a WT RT2 tumor) were plated on reconstituted ECM pre-processed with CM from cytokine-primed BMDMs. We found that CM from combined cytokine-treated BMDMs resulted in the highest enhancement of cancer cell invasion, whereas single-cytokine priming led to no significant alteration in invasion (Figure 7C). Considering the marked effect of T_H2-associated cytokines on cathepsin secretion, we used a pan-cathepsin inhibitor, JPM-OEt, to determine whether cathepsins are responsible for macrophage-mediated cancer cell invasion. Indeed, the addition of JPM-OEt abolished cancer cell invasion mediated by combined cytokine-treated BMDMs, indicating the crucial role of cathepsins in driving this process (Figure 7C). Moreover, the IRE1α inhibitor STF-083010 similarly impaired the ability of combined cytokine-stimulated BMDMs to promote tumor cell invasion (Figure 7C), which was likely caused by diminished cathepsin secretion. Taken together, our data demonstrate that T_H2-associated cytokines synergistically promote cathepsin secretion by macrophages in an IRE1α-dependent manner, which, in turn, facilitates cancer cell invasion.

DISCUSSION

Macrophages are capable of performing diverse functions in response to various signaling inputs. Previously, we showed that, in addition to its role in driving M2-like/alternative polarization, IL-4 upregulates cathepsin activities in TAMs to facilitate tumor development (Gocheva et al., 2010b). Here, using genetic strategies, we found that deletion of T_H2 cytokine signaling components in TAMs is sufficient to impair tumor growth and invasion in vivo, a finding that mirrored previous results where we showed that TAM-derived CtsB and CtsS played critical roles in RT2 tumor growth and invasion (Gocheva et al., 2010b). In the present study, we demonstrate that IL-4 cooperates with other cytokines—specifically, IL-6 and IL-10—to mediate the synergistic induction of cathepsin transcription and secretion in BMDMs. We found that the enhanced secretory phenotype of macrophages is concomitant with engagement of the UPR. Strikingly, transient knockdown and pharmacological inhibition of IRE1α led to a complete blockade in cathepsin secretion and a subsequent reduction in macrophage-mediated cancer cell invasion.

This study presents evidence for the first time that T_H2 cytokines and IRE1α regulate protease secretion from macrophages, an effect that was specific to the secretion of pro-form lysosomal proteases but not MMPs. This pro-form protease secretion suggests a potential re-routing of lysosomal proteases before they reach the lysosome, as we found no change in lysosomal function or acidification (data not shown). In contrast, previous reports demonstrated that interferon gamma (IFN-γ), an inducer of M1-like macrophage activation, increases the secretion of active-form CtsL (Beers et al., 2003). One explanation for this difference may be that combined T_H2 cytokine-treated macrophages upregulate CtsL and concomitantly downregulate the manose-6-phosphate (M6P) receptors *Igf2r* and *M6pr* (Table S1). This could lead to saturation of the M6P sorting system, whereby excess lysosomal enzymes are secreted into the extracellular space as pro-forms.

Moreover, it has been shown that the downstream effector of IRE1α, XBP1, controls the secretion of a subset of pro-inflammatory cytokines upon TLR2 or TLR4 ligation, which polarizes macrophages to an M1-like state (Martinon et al., 2010). Combined with our findings, these data suggest that the IRE1α/ XBP1 pathway may impact secretion across different macrophage polarization states, albeit with distinct outputs. It is also important to note that IRE1α/ XBP1 activation may not always be accompanied by a pronounced ER stress. In our studies, stimulation with combined cytokines induced classical ER stress targets (*Bip*, *Chop*, and *Pdi*) and activated PERK, but did not engage the ATF6 axis. Moreover, the magnitudes of such induction were significantly lower than those triggered by classical ER stress inducers, such as tunicamycin and thapsigargin.

These findings indicate that combined cytokine stimulation may instigate a low level of ER stress or perhaps no stress at all. Recently, $CD8a^+$ dendritic cells have been shown to engage the UPR in the absence of ER stress to mediate antigen cross-presentation (Osorio et al., 2014). Similar physiological engagement of the UPR has been identified in differentiating B cells where expansion of the ER is dependent upon ATF6 and IRE1α

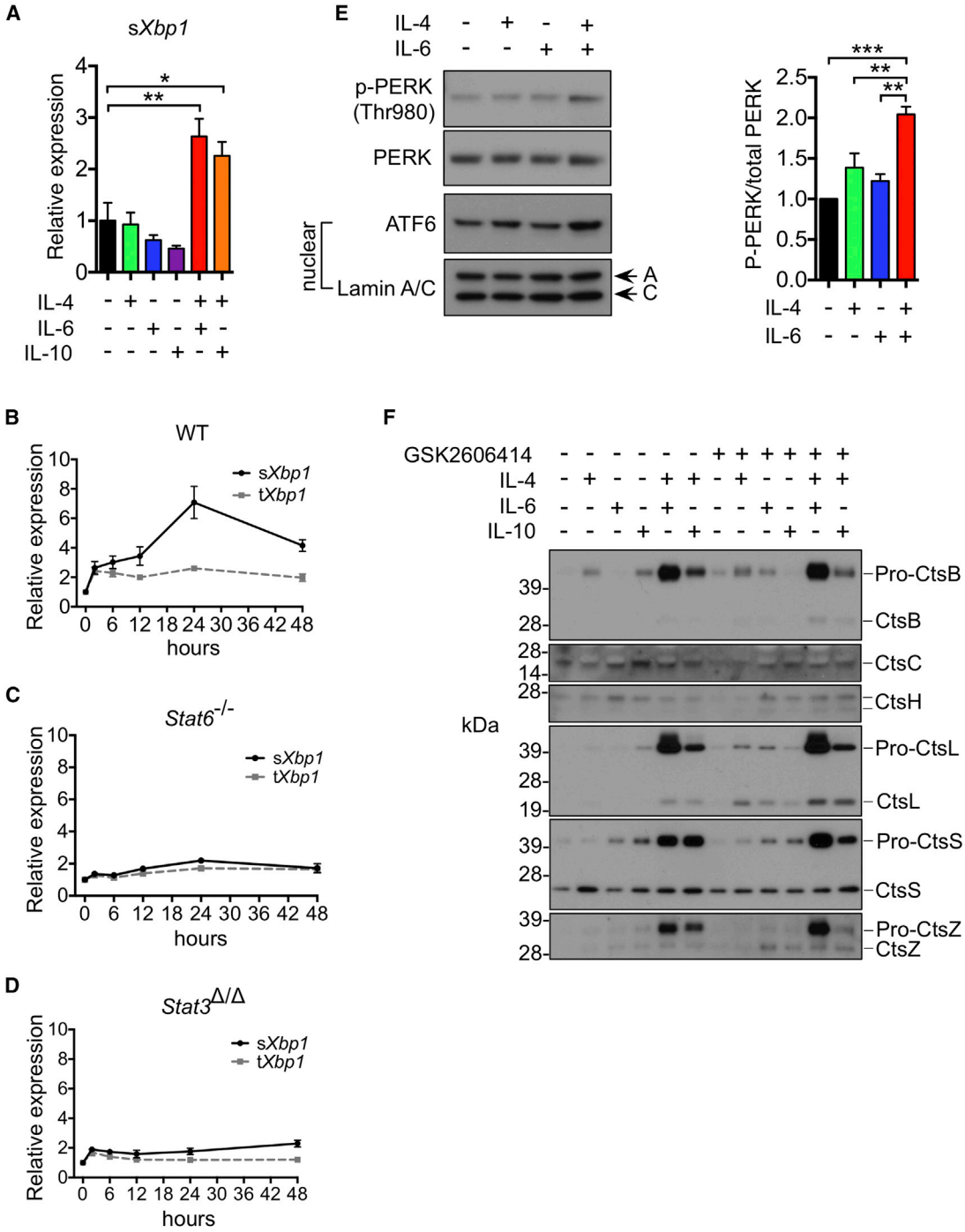

Figure 6. T_H2-Associated Cytokines Activate the UPR

(A) WT BMDMs were stimulated with IL-4, IL-6, IL-10, or their combinations for 24 hr. The level of spliced *Xbp1* (s*Xbp1*) mRNA was measured by qRT-PCR. Data are presented as mean ± SEM of n = 3 independent experiments.

(B–D) BMDMs from (B) WT, (C) *Stat6*$^{-/-}$, and (D) *Stat3*$^{\Delta/\Delta}$ mice were incubated with combined cytokines (IL-4 + IL-6) for up to 48 hr. s*Xbp1* and total *Xbp1* (t*Xbp1*) mRNA expression were quantified by qRT-PCR. Data are presented as mean ± SEM of n = 5 (WT) or n = 3 (*Stat6*$^{-/-}$ and *Stat3*$^{\Delta/\Delta}$) independent experiments.

(E) WT BMDMs were stimulated with the indicated cytokines for 24 hr, and whole-cell lysate (top two panels) or nuclear fraction (bottom two panels) was isolated for immunoblotting of phospho-PERK (p-PERK), total PERK, ATF6 (cleaved form), and Lamin A/C (left). Relative levels of phospho-PERK were quantified using total PERK as a normalization factor; data are presented as mean ± SEM of n = 3 independent experiments (right).

(legend continued on next page)

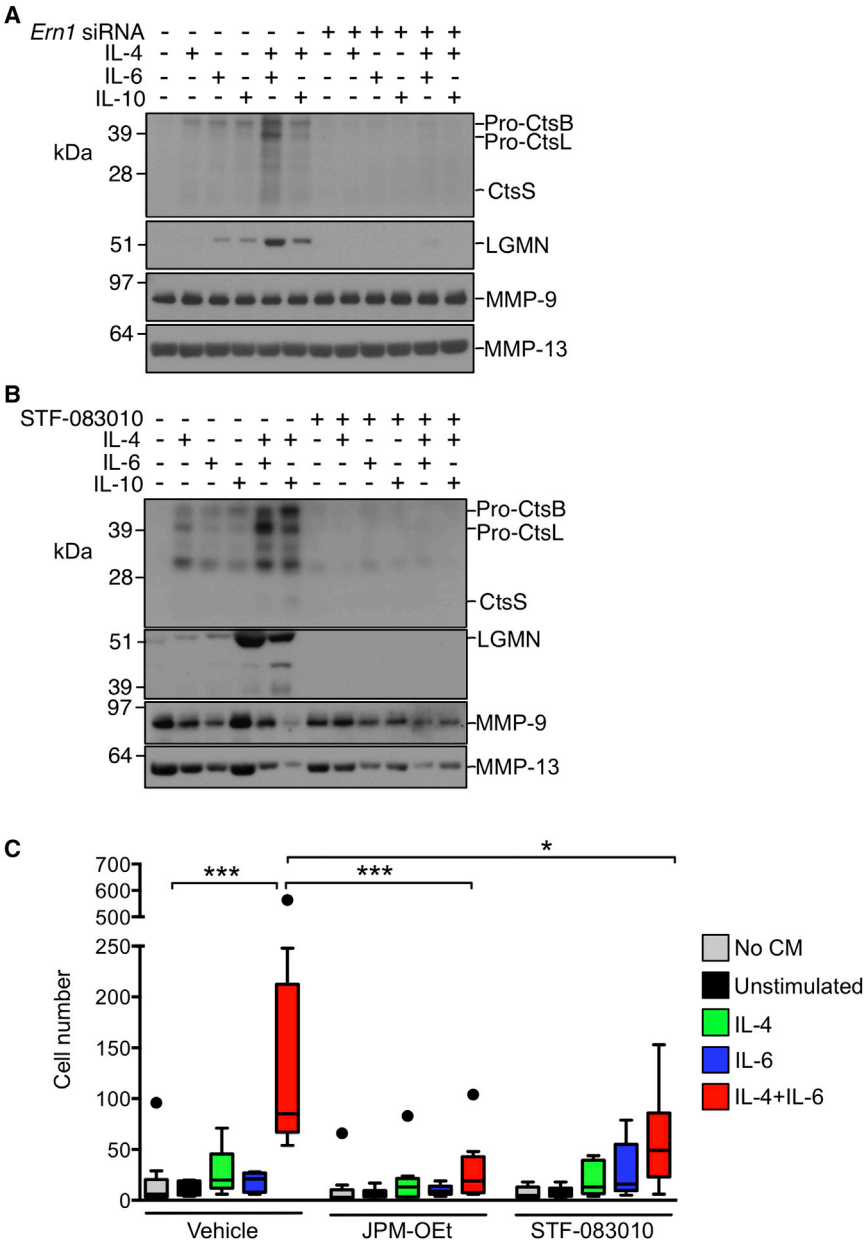

Figure 7. IRE1α Inhibition Blocks Cathepsin Secretion and Macrophage-Driven Cancer Cell Invasion

(A) BMDMs were incubated with pooled siRNA against *Ern1*, the gene encoding the IRE1α protein, or scrambled control siRNA and the indicated cytokines (10 ng/ml each) for 48 hr. Cells were then cultured under serum-free condition for 24 hr to generate conditioned media (CM). DCG-04-labeled CM was analyzed by immunoblotting for cathepsin abundance (top panel). Immunoblotting for legumain (LGMN), MMP9, and MMP13 proteins was also performed using unlabeled CM (lower panels).

(B) BMDMs were incubated with individual or combinatorial cytokines, in the presence or absence of the IRE1α inhibitor STF-083010 (100 μM) for 48 hr. As in (A), CM was assayed for secretion of cathepsins, LGMN, MMP9, and MMP13. Protein sizes (in kilodaltons) are indicated on the left of each blot.

(C) CM were prepared from BMDMs treated with the indicated cytokines in the presence or absence of STF-083010. CM were activated in cathepsin activation buffer and then applied onto Matrigel-coated FluoroBlok inserts in the presence or absence of the pan-cathepsin inhibitor JPM-OEt (100 μM). After 24 hr of matrix processing, βTC374 cancer cells were plated onto the inserts, and cell invasion proceeded for 48 hr. The level of invasion in each condition was quantified by counting the number of $DAPI^+$ cancer cells. Data from n = 9 independent experiments are shown as Tukey box-and-whisker plots, with values outside the whiskers. All data points were included in statistical analyses. Ordinary one-way ANOVA with Holm-Sidak's multiple comparisons test was used for statistical analysis. *$p < 0.05$; ***$p < 0.001$.

See also Figure S7.

and, importantly, precedes the production of immunoglobulin (Iwakoshi et al., 2003; van Anken et al., 2003). In addition, thyroid-stimulating hormone-stimulated thyrocytes activate the UPR preemptively to maintain thyroglobulin secretion (Christis et al., 2010). In light of these reports, our data suggest that macrophages stimulated with IL-4 and IL-6/ IL-10 may engage the IRE1α/XBP1 pathway to mediate the secretory load of lysosomal proteases.

Our results also emphasize cathepsin protease production as a functional aspect of the tumor-promoting TAM phenotype. We previously found that cathepsin activity increases during the course of disease progression in PanNETs and breast cancer and that TAM-supplied cathepsins substantially contribute to tumor growth, invasion, and angiogenesis in a PanNET mouse model, with the highest level of cathepsin activity present in invasive IC2 tumors (Gocheva et al., 2010b). In concordance with previous reports showing IL-6-mediated transcriptional control of *CtsB* (Mohamed et al., 2010), our data herein indicate that cathepsin production in TAMs is, at least partially, regulated by a group of T_H2-associated cytokines, which are abundant in the PanNET TME. These results also represent an

(F) BMDMs from WT mice were treated with the indicated cytokines and with a PERK inhibitor GSK2606414 (500 nM) or vehicle (DMSO) for 48 hr. CM were then collected and immunoblotted for CtsB, CtsC, CtsH, CtsL, CtsS, and CtsZ. Protein sizes (in kilodaltons) are indicated on the left of each blot. Ordinary one-way ANOVA with Holm-Sidak's multiple comparisons test was used for statistical analysis. *$p < 0.05$; **$p < 0.01$; ***$p < 0.001$. See also Figures S5 and S6.

interesting comparison with the report that lipopolysaccharide (LPS)-stimulated macrophages robustly upregulate a variety of M1-associated cytokines, including CXCL1 and IL-1β, but not cathepsins (Meissner et al., 2013). Therefore, we propose that a high level of pro-form cathepsin secretion is a characteristic of M2-like macrophages, such as TAMs, and that extracellular cathepsin-mediated proteolysis coordinates with other TAM-mediated processes, such as immunosuppression and angiogenesis, to promote tumor development.

In conclusion, we have demonstrated that complementary T_H2-associated cytokines lead to a distinct macrophage activation state characterized by a robust secretory capacity. These cytokines engage a non-canonical IRE1α axis to promote cathepsin secretion, thus promoting tumor progression and invasion. Given that several cathepsin inhibitors have minimal toxicities (Palermo and Joyce, 2008) and deliver therapeutic efficacy in preclinical PanNET models (Joyce et al., 2004; Elie et al., 2010), our findings further emphasize the potential of cathepsin inhibition as a therapeutic strategy in pancreatic neuroendocrine tumors and other cancers.

EXPERIMENTAL PROCEDURES

Mice, Cell Lines, and Pharmacological Inhibitors

The generation of RT2 (Hanahan, 1985), *Il4ra*$^{-/-}$ (Noben-Trauth et al., 1997), *Stat6*$^{-/-}$ (Kaplan et al., 1996), *LysM*:Cre (Clausen et al., 1999), and *Stat3*$^{Flox/Flox}$ (Takeda et al., 1998) mice have been reported previously. The *Il4ra*$^{-/-}$ and *Stat6*$^{-/-}$ mice were purchased from Jackson Laboratories. *LysM:*Cre and *Stat3*$^{Flox/Flox}$ mice were obtained from Dr. Alexander Rudensky. The *Il4ra*$^{-/-}$ mice, which were originally in the BALB/c background, were backcrossed into the C57BL/6 background for ten generations. All mouse strains were maintained in the C57BL/6 background. The animal studies were approved by the Institutional Animal Care and Use Committee at Memorial Sloan Kettering Cancer Center (MSKCC). The βTC374 cancer cell line was derived from a WT RT2 tumor in the J.A.J. lab. The following inhibitors were commercially available: STF-083010 (EMD Millipore), GSK2606414 (Tocris), KIRA6 (Calbiochem), and 4μ8C (Selleckchem). The pan-cathepsin inhibitor JPM-OEt was synthesized by the Organic Synthesis core at MSKCC.

Tumor Volume Measurement and Invasion Analysis

Tumor burden was determined at 13.5 weeks of age for RT2 mice of all genotypes. For invasion grading, stained pancreatic tissues were graded as previously described (Lopez and Hanahan, 2002; Gocheva et al., 2010b). For more details, see the Supplemental Experimental Procedures.

Flow Cytometry and FACS

A single-cell suspension from RT2 tumors was stained with the antibodies summarized in Table S2. A BD LSR II flow cytometer was used for data acquisition, and data were analyzed using FlowJo software. For cell sorting, samples were sorted on a FACSAria II or MoFlo cell sorter. For more details, see the Supplemental Experimental Procedures.

RNA Isolation and qRT-PCR

RNA was isolated using the TRIzol/chloroform method (Invitrogen), and first-strand cDNA was synthesized using the High-Capacity cDNA Reverse Transcription Kit (Invitrogen). For more details, see the Supplemental Experimental Procedures.

Derivation and Culture of BMDMs

BM was harvested from WT, *Stat6*$^{-/-}$, and *LysM:Cre; Stat3*$^{Flox/Flox}$ mice. BM-derived cells were cultured for 7 days to generate mature macrophages. For more details on cell culture and cell-based assays, see the Supplemental Experimental Procedures.

DCG-04 Labeling and Western Blotting

Biotinylated DCG-04 (Greenbaum et al., 2002) was synthesized by the Organic Synthesis Core Facility at MSKCC. Labeling was performed at room temperature. For western blotting, samples were resolved in NuPAGE SDS-PAGE gels (Invitrogen), transferred to polyvinylidene fluoride (PVDF) membranes, and detected using chemiluminescence (Thermo Fisher Scientific). For IRE1α activation analysis, Phos-tag SDS-PAGE (Wako) was performed. For more details, see the Supplemental Experimental Procedures.

Knockdown of IRE1α in BMDMs

BMDMs were transfected with pooled siRNA against *Ern1*, the gene encoding IRE1α (Dharmacon), or scrambled siRNA (Invitrogen), using Viromer BLUE (Lipocalyx). For more details, see the Supplemental Experimental Procedures.

Microarray and Computational Analysis

Sample Generation

BMDMs were generated as described earlier. On day 7, BMDMs were treated with control media, IL-4, IL-6, IL-10, IL-4 + IL-6, or IL-4 + IL-10 for 24 hr (all cytokines were used at 10 ng/ml; CSF-1 was supplemented at 10 ng/ml). Cells were harvested and lysed in TRIzol. RNA isolation, library preparation, and pre-processing were completed by the MSKCC Genomics Core Facility using Affymetrix Mouse 430A 2.0 microarrays. All downstream bioinformatic analyses were completed in R 3.0.1 using the Bioconductor suite of packages. Differentially expressed genes were identified using the "limma" package (Ritchie et al., 2015), with a fold change cutoff of ±2 and a false discovery rate (FDR) of 10%. These cutoffs were used to identify synergistic and antagonistic genes in the interaction-based linear model described here:

$$\text{Expression}_{\text{Gene}} = \text{baseline}_{\text{Gene}} + [\text{IL-4}] * \beta_{\text{IL-4_Gene}} + [\text{IL-6}] * \beta_{\text{IL-6_Gene}} + [\text{IL-10}] * \beta_{\text{IL-10_Gene}} + [\text{IL-4}][\text{IL-6}] * \beta_{\text{IL-4+IL-6_Gene}} + [\text{IL-4}][\text{IL-10}] * \beta_{\text{IL-4+IL-10_Gene}}.$$

Linear model coefficients plotted in Figures 5A and S4C were normalized to baseline for each gene. GO analysis was performed with iPAGE, and motif activity response analysis (MARA) was performed at http://ismara.unibas.ch/fcgi/mara; additional details can be found in the Supplemental Experimental Procedures.

Statistical Analysis and Plotting

Data are presented throughout as mean ± SEM, analyzed by the indicated tests with a significance cutoff of $p < 0.05$. All statistical analyses were completed in GraphPad Prism 6.0 and R 3.0.1. All tumor volume box-and-whisker plots are drawn as Tukey boxplots, with upper whiskers extending to the 75% value multiplied by 1.5× the inter-quartile range and lower whiskers extending to the 25% value multiplied by 1.5× the inter-quartile range (GraphPad Prism default Tukey options). All plotted data points were included in subsequent statistical analyses as described in the figure legends. All code used to analyze the data can be found at the following website: https://bitbucket.org/bowmanr/joycelab-macrophage. For more details, see the Supplemental Experimental Procedures.

ACCESSION NUMBERS

The accession number for the raw microarray data reported in this paper is GEO: GSE70626.

SUPPLEMENTAL INFORMATION

Supplemental Information includes Supplemental Experimental Procedures, seven figures, and three tables and can be found with this article online at http://dx.doi.org/10.1016/j.celrep.2016.08.035.

AUTHOR CONTRIBUTIONS

D.Y., H.-W.W., R.L.B., and J.A.J designed experiments and analyzed data. D.Y., H.-W.W., and R.L.B. performed experiments. R.L.B. performed

computational analyses. J.A.J. conceived and supervised the study. D.Y., R.L.B., and J.A.J. wrote the manuscript.

ACKNOWLEDGMENTS

We thank Xiaoping Chen and Kenishana Simpson for excellent technical support and Claire Hamilton for assistance with the *Stat6* null mouse experiments. We thank members of the J.A.J. lab for insightful comments and discussion. We are grateful for help from Elyn Reidel, the MSKCC Biostatistics Department for assistance with statistical analyses of tumor invasion. We thank Dr. Alexander Rudensky for generously providing the *Stat3*$^{Flox/Flox}$ and *LysM*:Cre animals. This research was supported by the American Cancer Society (121839-RSG-12-076-01-LIB to J.A.J.), a National Cancer Institute Cancer Center support grant (P30 CA008748 awarded to MSKCC), a National Cancer Institute fellowship (5F31CA167863 to R.L.B.), and the graduate training programs of the Weill Cornell Medical School (to H.-W.W.) and the Gerstner Sloan-Kettering Graduate School (to R.L.B.).

Received: February 23, 2016
Revised: July 13, 2016
Accepted: August 11, 2016
Published: September 13, 2016

REFERENCES

Akkari, L., Gocheva, V., Kester, J.C., Hunter, K.E., Quick, M.L., Sevenich, L., Wang, H.W., Peters, C., Tang, L.H., Klimstra, D.S., et al. (2014). Distinct functions of macrophage-derived and cancer cell-derived cathepsin Z combine to promote tumor malignancy via interactions with the extracellular matrix. Genes Dev. *28*, 2134–2150.

Akkari, L., Gocheva, V., Quick, M.L., Kester, J.C., Spencer, A.K., Garfall, A.L., Bowman, R.L., and Joyce, J.A. (2016). Combined deletion of cathepsin protease family members reveals compensatory mechanisms in cancer. Genes Dev. *30*, 220–232.

Beers, C., Honey, K., Fink, S., Forbush, K., and Rudensky, A. (2003). Differential regulation of cathepsin S and cathepsin L in interferon gamma-treated macrophages. J. Exp. Med. *197*, 169–179.

Bettigole, S.E., and Glimcher, L.H. (2015). Endoplasmic reticulum stress in immunity. Annu. Rev. Immunol. *33*, 107–138.

Biswas, S.K., and Mantovani, A. (2010). Macrophage plasticity and interaction with lymphocyte subsets: cancer as a paradigm. Nat. Immunol. *11*, 889–896.

Chandramohanadas, R., Davis, P.H., Beiting, D.P., Harbut, M.B., Darling, C., Velmourougane, G., Lee, M.Y., Greer, P.A., Roos, D.S., and Greenbaum, D.C. (2009). Apicomplexan parasites co-opt host calpains to facilitate their escape from infected cells. Science *324*, 794–797.

Christis, C., Fullaondo, A., Schildknegt, D., Mkrtchian, S., Heck, A.J., and Braakman, I. (2010). Regulated increase in folding capacity prevents unfolded protein stress in the ER. J. Cell Sci. *123*, 787–794.

Clausen, B.E., Burkhardt, C., Reith, W., Renkawitz, R., and Förster, I. (1999). Conditional gene targeting in macrophages and granulocytes using LysMcre mice. Transgenic Res. *8*, 265–277.

El Chartouni, C., Schwarzfischer, L., and Rehli, M. (2010). Interleukin-4 induced interferon regulatory factor (Irf) 4 participates in the regulation of alternative macrophage priming. Immunobiology *215*, 821–825.

Elie, B.T., Gocheva, V., Shree, T., Dalrymple, S.A., Holsinger, L.J., and Joyce, J.A. (2010). Identification and pre-clinical testing of a reversible cathepsin protease inhibitor reveals anti-tumor efficacy in a pancreatic cancer model. Biochimie *92*, 1618–1624.

Gocheva, V., Zeng, W., Ke, D., Klimstra, D., Reinheckel, T., Peters, C., Hanahan, D., and Joyce, J.A. (2006). Distinct roles for cysteine cathepsin genes in multistage tumorigenesis. Genes Dev. *20*, 543–556.

Gocheva, V., Chen, X., Peters, C., Reinheckel, T., and Joyce, J.A. (2010a). Deletion of cathepsin H perturbs angiogenic switching, vascularization and growth of tumors in a mouse model of pancreatic islet cell cancer. Biol. Chem. *391*, 937–945.

Gocheva, V., Wang, H.W., Gadea, B.B., Shree, T., Hunter, K.E., Garfall, A.L., Berman, T., and Joyce, J.A. (2010b). IL-4 induces cathepsin protease activity in tumor-associated macrophages to promote cancer growth and invasion. Genes Dev. *24*, 241–255.

Goodarzi, H., Elemento, O., and Tavazoie, S. (2009). Revealing global regulatory perturbations across human cancers. Mol. Cell *36*, 900–911.

Greenbaum, D., Medzihradszky, K.F., Burlingame, A., and Bogyo, M. (2000). Epoxide electrophiles as activity-dependent cysteine protease profiling and discovery tools. Chem. Biol. *7*, 569–581.

Greenbaum, D.C., Arnold, W.D., Lu, F., Hayrapetian, L., Baruch, A., Krumrine, J., Toba, S., Chehade, K., Brömme, D., Kuntz, I.D., and Bogyo, M. (2002). Small molecule affinity fingerprinting. A tool for enzyme family subclassification, target identification, and inhibitor design. Chem. Biol. *9*, 1085–1094.

Hanahan, D. (1985). Heritable formation of pancreatic beta-cell tumours in transgenic mice expressing recombinant insulin/simian virus 40 oncogenes. Nature *315*, 115–122.

Hiwatashi, K., Tamiya, T., Hasegawa, E., Fukaya, T., Hashimoto, M., Kakoi, K., Kashiwagi, I., Kimura, A., Inoue, N., Morita, R., et al. (2011). Suppression of SOCS3 in macrophages prevents cancer metastasis by modifying macrophage phase and MCP2/CCL8 induction. Cancer Lett. *308*, 172–180.

Hornung, V., Bauernfeind, F., Halle, A., Samstad, E.O., Kono, H., Rock, K.L., Fitzgerald, K.A., and Latz, E. (2008). Silica crystals and aluminum salts activate the NALP3 inflammasome through phagosomal destabilization. Nat. Immunol. *9*, 847–856.

Iwakoshi, N.N., Lee, A.H., Vallabhajosyula, P., Otipoby, K.L., Rajewsky, K., and Glimcher, L.H. (2003). Plasma cell differentiation and the unfolded protein response intersect at the transcription factor XBP-1. Nat. Immunol. *4*, 321–329.

Joyce, J.A., Baruch, A., Chehade, K., Meyer-Morse, N., Giraudo, E., Tsai, F.Y., Greenbaum, D.C., Hager, J.H., Bogyo, M., and Hanahan, D. (2004). Cathepsin cysteine proteases are effectors of invasive growth and angiogenesis during multistage tumorigenesis. Cancer Cell *5*, 443–453.

Kaplan, M.H., Schindler, U., Smiley, S.T., and Grusby, M.J. (1996). Stat6 is required for mediating responses to IL-4 and for development of Th2 cells. Immunity *4*, 313–319.

Lopez, T., and Hanahan, D. (2002). Elevated levels of IGF-1 receptor convey invasive and metastatic capability in a mouse model of pancreatic islet tumorigenesis. Cancer Cell *1*, 339–353.

Martinon, F., Chen, X., Lee, A.H., and Glimcher, L.H. (2010). TLR activation of the transcription factor XBP1 regulates innate immune responses in macrophages. Nat. Immunol. *11*, 411–418.

Mauer, J., Chaurasia, B., Goldau, J., Vogt, M.C., Ruud, J., Nguyen, K.D., Theurich, S., Hausen, A.C., Schmitz, J., Brönneke, H.S., et al. (2014). Signaling by IL-6 promotes alternative activation of macrophages to limit endotoxemia and obesity-associated resistance to insulin. Nat. Immunol. *15*, 423–430.

Meissner, F., Scheltema, R.A., Mollenkopf, H.J., and Mann, M. (2013). Direct proteomic quantification of the secretome of activated immune cells. Science *340*, 475–478.

Mohamed, M.M., Cavallo-Medved, D., Rudy, D., Anbalagan, A., Moin, K., and Sloane, B.F. (2010). Interleukin-6 increases expression and secretion of cathepsin B by breast tumor-associated monocytes. Cell. Physiol. Biochem. *25*, 315–324.

Noben-Trauth, N., Shultz, L.D., Brombacher, F., Urban, J.F., Jr., Gu, H., and Paul, W.E. (1997). An interleukin 4 (IL-4)-independent pathway for CD4+ T cell IL-4 production is revealed in IL-4 receptor-deficient mice. Proc. Natl. Acad. Sci. USA *94*, 10838–10843.

Noy, R., and Pollard, J.W. (2014). Tumor-associated macrophages: from mechanisms to therapy. Immunity *41*, 49–61.

Olson, O.C., and Joyce, J.A. (2015). Cysteine cathepsin proteases: regulators of cancer progression and therapeutic response. Nat. Rev. Cancer *15*, 712–729.

Osorio, F., Tavernier, S.J., Hoffmann, E., Saeys, Y., Martens, L., Vetters, J., Delrue, I., De Rycke, R., Parthoens, E., Pouliot, P., et al. (2014). The unfolded-protein-response sensor IRE-1α regulates the function of CD8α+ dendritic cells. Nat. Immunol. *15*, 248–257.

Ostuni, R., Piccolo, V., Barozzi, I., Polletti, S., Termanini, A., Bonifacio, S., Curina, A., Prosperini, E., Ghisletti, S., and Natoli, G. (2013). Latent enhancers activated by stimulation in differentiated cells. Cell *152*, 157–171.

Palermo, C., and Joyce, J.A. (2008). Cysteine cathepsin proteases as pharmacological targets in cancer. Trends Pharmacol. Sci. *29*, 22–28.

Papandreou, I., Denko, N.C., Olson, M., Van Melckebeke, H., Lust, S., Tam, A., Solow-Cordero, D.E., Bouley, D.M., Offner, F., Niwa, M., and Koong, A.C. (2011). Identification of an Ire1alpha endonuclease specific inhibitor with cytotoxic activity against human multiple myeloma. Blood *117*, 1311–1314.

Qian, B.Z., and Pollard, J.W. (2010). Macrophage diversity enhances tumor progression and metastasis. Cell *141*, 39–51.

Quail, D.F., and Joyce, J.A. (2013). Microenvironmental regulation of tumor progression and metastasis. Nat. Med. *19*, 1423–1437.

Reimold, A.M., Iwakoshi, N.N., Manis, J., Vallabhajosyula, P., Szomolanyi-Tsuda, E., Gravallese, E.M., Friend, D., Grusby, M.J., Alt, F., and Glimcher, L.H. (2001). Plasma cell differentiation requires the transcription factor XBP-1. Nature *412*, 300–307.

Riese, R.J., Wolf, P.R., Brömme, D., Natkin, L.R., Villadangos, J.A., Ploegh, H.L., and Chapman, H.A. (1996). Essential role for cathepsin S in MHC class II-associated invariant chain processing and peptide loading. Immunity *4*, 357–366.

Ritchie, M.E., Phipson, B., Wu, D., Hu, Y., Law, C.W., Shi, W., and Smyth, G.K. (2015). limma powers differential expression analyses for RNA-sequencing and microarray studies. Nucleic Acids Res. *43*, e47.

Rooney, H.C., Van't Klooster, J.W., van der Hoorn, R.A., Joosten, M.H., Jones, J.D., and de Wit, P.J. (2005). Cladosporium Avr2 inhibits tomato Rcr3 protease required for Cf-2-dependent disease resistance. Science *308*, 1783–1786.

Ruffell, B., and Coussens, L.M. (2015). Macrophages and therapeutic resistance in cancer. Cancer Cell *27*, 462–472.

Shiao, S.L., Ganesan, A.P., Rugo, H.S., and Coussens, L.M. (2011). Immune microenvironments in solid tumors: new targets for therapy. Genes Dev. *25*, 2559–2572.

Stritesky, G.L., Muthukrishnan, R., Sehra, S., Goswami, R., Pham, D., Travers, J., Nguyen, E.T., Levy, D.E., and Kaplan, M.H. (2011). The transcription factor STAT3 is required for T helper 2 cell development. Immunity *34*, 39–49.

Suzuki, H., Forrest, A.R., van Nimwegen, E., Daub, C.O., Balwierz, P.J., Irvine, K.M., Lassmann, T., Ravasi, T., Hasegawa, Y., de Hoon, M.J., et al.; FANTOM Consortium; Riken Omics Science Center (2009). The transcriptional network that controls growth arrest and differentiation in a human myeloid leukemia cell line. Nat. Genet. *41*, 553–562.

Takeda, K., Noguchi, K., Shi, W., Tanaka, T., Matsumoto, M., Yoshida, N., Kishimoto, T., and Akira, S. (1997). Targeted disruption of the mouse Stat3 gene leads to early embryonic lethality. Proc. Natl. Acad. Sci. USA *94*, 3801–3804.

Takeda, K., Kaisho, T., Yoshida, N., Takeda, J., Kishimoto, T., and Akira, S. (1998). Stat3 activation is responsible for IL-6-dependent T cell proliferation through preventing apoptosis: generation and characterization of T cell-specific Stat3-deficient mice. J. Immunol. *161*, 4652–4660.

Takeda, K., Clausen, B.E., Kaisho, T., Tsujimura, T., Terada, N., Förster, I., and Akira, S. (1999). Enhanced Th1 activity and development of chronic enterocolitis in mice devoid of Stat3 in macrophages and neutrophils. Immunity *10*, 39–49.

Turk, V., Stoka, V., Vasiljeva, O., Renko, M., Sun, T., Turk, B., and Turk, D. (2012). Cysteine cathepsins: from structure, function and regulation to new frontiers. Biochim. Biophys. Acta *1824*, 68–88.

van Anken, E., Romijn, E.P., Maggioni, C., Mezghrani, A., Sitia, R., Braakman, I., and Heck, A.J. (2003). Sequential waves of functionally related proteins are expressed when B cells prepare for antibody secretion. Immunity *18*, 243–253.

Vasiljeva, O., Papazoglou, A., Krüger, A., Brodoefel, H., Korovin, M., Deussing, J., Augustin, N., Nielsen, B.S., Almholt, K., Bogyo, M., et al. (2006). Tumor cell-derived and macrophage-derived cathepsin B promotes progression and lung metastasis of mammary cancer. Cancer Res. *66*, 5242–5250.

Wang, H.W., and Joyce, J.A. (2010). Alternative activation of tumor-associated macrophages by IL-4: priming for protumoral functions. Cell Cycle *9*, 4824–4835.

Wiley, H.S., VanNostrand, W., McKinley, D.N., and Cunningham, D.D. (1985). Intracellular processing of epidermal growth factor and its effect on ligand-receptor interactions. J. Biol. Chem. *260*, 5290–5295.